

## Shear-induced vortex decoupling in $\text{Bi}_2\text{Sr}_2\text{CaCu}_2\text{O}_8$ crystals

B. Khaykovich, D. T. Fuchs,\* K. Teitelbaum, Y. Myasoedov, and E. Zeldov  
*Department of Condensed Matter Physics, Weizmann Institute of Science, 76100 Rehovot, Israel*

T. Tamegai and S. Ooi†  
*Department of Applied Physics, The University of Tokyo, Hongo, Bunkyo-ku, Tokyo 113-8656, Japan*

M. Konczykowski  
*CNRS, UMR 7642, Laboratoire des Solides Irradies, Ecole Polytechnique, 91128 Palaiseau, France*

R. A. Doyle and S. F. W. R. Rycroft  
*IRC in Superconductivity, University of Cambridge, Cambridge CB3 0HE, United Kingdom*  
 (Received 4 January 2000)

Simultaneous transport and magnetization studies in  $\text{Bi}_2\text{Sr}_2\text{CaCu}_2\text{O}_8$  crystals at elevated currents reveal large discrepancies, including *finite* resistivity at temperatures of 40 K *below* the magnetic irreversibility line. This resistivity, measured at the top surface, is nonmonotonic in temperature and extremely nonlinear. The vortex velocity derived from magnetization is six orders of magnitude lower than the velocity derived from *simultaneous* transport measurements. The findings are ascribed to a shear-induced decoupling, in which the pancake vortices flow only in the top few  $\text{CuO}_2$  planes, and are decoupled from the pinned vortices in the rest of the crystal.

Transport measurements are one of the most common methods to study vortex dynamics in superconductors. The derived resistivity  $\rho$  describes the vortex motion as a function of temperature, field, and the applied current. In high-temperature superconductors the situation is more complicated due to their high anisotropy and layered structure. The corresponding resistivity has two main components, the in-plane resistivity  $\rho_{ab}$  and the out-of-plane  $\rho_c$ , with typical ratio of  $\rho_c/\rho_{ab} \approx 10^4$  in the normal state of  $\text{Bi}_2\text{Sr}_2\text{CaCu}_2\text{O}_8$  (BSCCO) crystals.<sup>1</sup> As a result, the measured resistance  $R$  is a nontrivial function of sample geometry and contact configuration,<sup>1,2</sup> which is further significantly complicated by the nonlinear current dependence of  $\rho_{ab}$  and  $\rho_c$ . Yet it is generally assumed that the physical mechanism that governs the dissipation can be described in terms of current density, namely, the local values of  $\rho_{ab}$  and  $\rho_c$  are determined<sup>3,4</sup> by the corresponding in-plane and out-of-plane current densities  $j_{ab}$  and  $j_c$  (ignoring possible nonlocal effects<sup>5,6</sup>). In this paper we demonstrate that in highly anisotropic materials such as BSCCO this assumption may not be valid. We find that at elevated currents an additional term, the  $c$  axis *gradient* of the in-plane current  $dj_{ab}/dz$ , becomes the dominant parameter in the description of the local dissipation. This current gradient induces large velocity gradients  $dv_{ab}/dz$  of the pancake vortices in the different  $\text{CuO}_2$  planes, leading to their decoupling and to corresponding dramatic increase in  $\rho_c$  and anisotropy  $\gamma$ . In the presence of inhomogeneous currents, this mechanism results in fundamental changes in the transport behavior, including large measurable reentrant resistance  $R(T)$  well *below* the magnetically determined irreversibility line (IL).

The studies were carried out on several high quality BSCCO crystals,<sup>7</sup> with  $T_c \approx 90$  K. Four wires were attached to the gold pads evaporated on freshly cleaved top  $ab$  sur-

faces, as shown schematically in the inset to Fig. 1(a). The bottom surface of the crystals, free of electrical contacts, was attached to an array of 19 2DEG Hall sensors,<sup>8</sup>  $30 \times 30 \mu\text{m}^2$  each, allowing *simultaneous* resistance and local magnetization measurements in the presence of transport current. In addition, several crystals were irradiated by very low doses of 5.8 GeV Pb ions to produce columnar defects with concentrations corresponding to matching fields of  $B_\phi = 5, 20, \text{ and } 60$  G. In order to focus on bulk vortex dynamics and to avoid complications due to surface barriers,<sup>9</sup> most of the samples were prepared in a form of large square platelets with electrical contacts positioned far from the edges.<sup>10</sup> Some of the crystals were cut into strip shape for comparison. Although detailed behavior varies from sample to sample, the qualitative features described below were observed in all the samples regardless of the surface barriers and the irradiation doses. Here we present data for as-grown crystal A of size  $1700 \times 1300 \times 10 \mu\text{m}^3$ , which was subsequently cut into a strip, and for an irradiated crystal B  $1000 \times 700 \times 30 \mu\text{m}^3$  with  $B_\phi = 60$  G.

Our main general observation is displayed in Fig. 1. Figure 1(a) shows the  $R(T)$  of the unirradiated crystal A at various applied fields  $H_{\parallel} \parallel c$  axis at elevated applied current of 30 mA. At lower currents, that are usually used in transport studies,  $R(T)$  behaves monotonically with temperature as shown for comparison by the dashed line in Fig. 1(a) for 10 mA at 500 Oe. However, when  $I_a$  is increased we find surprisingly a very pronounced reentrant behavior, in which  $R(T)$  reaches a minimum at some characteristic temperature  $T_{min}$ , but then increases again, often by more than an order of magnitude, at lower  $T$ . At 100 Oe a sharp drop in  $R(T)$  is observed at the first-order melting transition (FOT),  $T_m$ , followed by a monotonic resistive tail in the quasi-ordered-lattice phase, as described previously.<sup>10</sup> At 200 Oe the be-

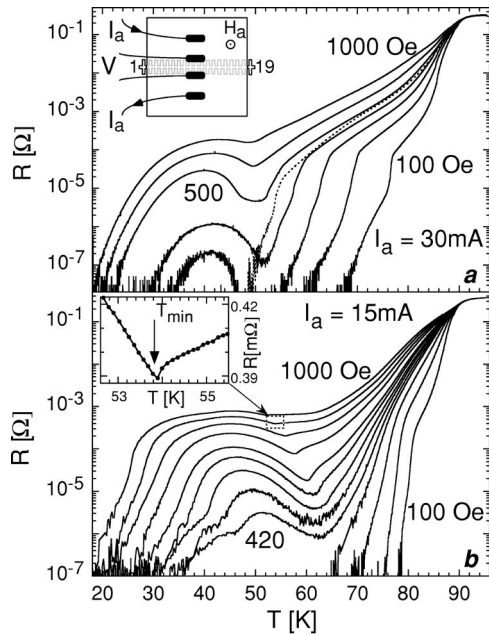


FIG. 1.  $R$  (log scale) vs  $T$  at various applied fields. (a) As-grown sample A at 100, 200, 300, 400, 500, 700, and 1000 Oe;  $I_a = 30$  mA. Dashed line: 500 Oe and 10 mA. Inset: schematic sample configuration with Hall sensors underneath. (b) Irradiated sample B at 100, 200, 300, 380, 420, 460, 500, 550, 600, 700, 800, 900, and 1000 Oe;  $I_a = 15$  mA. Inset to (b) shows  $R(T)$  in the vicinity of  $T_{min}$  at 900 Oe on linear scale.

havior is still monotonic similar to 100 Oe data. At 300 Oe, however,  $R(T)$  decreases monotonically down to our noise level at about 55 K, but then reappears again between 46 and 34 K. This reentrant behavior is strongly pronounced at 400 Oe and up to fields above 1000 Oe. In addition, a sharp discontinuity in the derivative  $dR(T)/dT$  is often observed at  $T_{min}$  as shown in the inset to Fig. 1(b). The irradiated samples display essentially similar properties, as shown in Fig. 1(b), with a few consistent differences: (i) The resistive kink at the FOT is smeared by the low dose of columnar defects, consistent with previous studies,<sup>11</sup> (ii)  $T_{min}$  is generally shifted to higher temperatures, and (iii) the anomalous behavior appears at lower currents, as shown by the 15 mA data in Fig. 1(b). The general form of  $R(T)$  in Fig. 1 is somewhat reminiscent of the ‘‘peak effect’’ observed<sup>12</sup> in NbSe<sub>2</sub> near  $H_{c2}$ , or at the melting transition<sup>13</sup> in YBa<sub>2</sub>Cu<sub>3</sub>O<sub>7</sub>. The behavior reported here, however, is much broader and is of a fundamentally different nature.

In the unirradiated crystals the reentrant features usually appear above 25 mA, close to our upper bound of 30 mA, limited by the contact resistance. The enhanced pinning in the irradiated samples causes the anomalous behavior to begin at  $I_a$  as low as 10 mA, allowing a more systematic study. Figures 2(a) and 2(b) thus present  $R(T)$  of crystal B at various  $I_a$  at 200 and 500 Oe, respectively. At low currents  $R(T)$  is monotonic and only weakly current dependent, and has a rather well-defined temperature  $T_{R=0}$  at which  $R(T)$  drops below experimental resolution. All these qualities change drastically at higher currents. The appearance of nonmonotonic  $R(T)$  is accompanied by extreme nonlinearity. An increase of  $I_a$  by 30% or less may result in enhancement of  $R$  by orders of magnitude. Furthermore, the same current in-

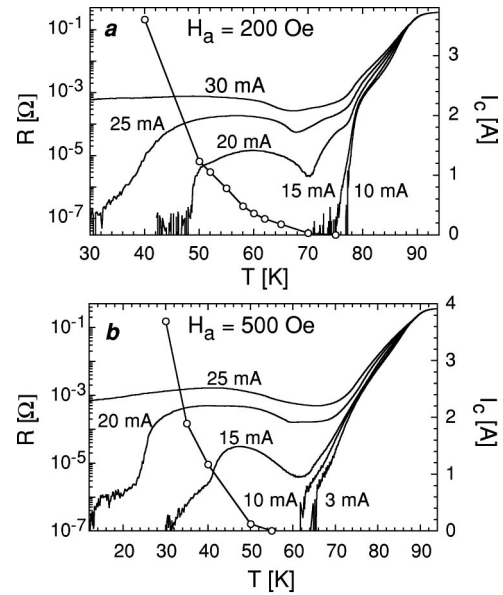


FIG. 2. Resistance at various  $I_a$  (left axis, log scale) and magnetically measured critical current (right axis, linear scale, open circles) vs  $T$  for the irradiated sample,  $H_a = 200$  Oe (a) and  $H_a = 500$  Oe (b).

crease causes a decrease of  $T_{R=0}$  by tens of degrees K.

In order to elucidate the origin of this anomalous behavior we have carried out simultaneous local magnetization measurements *in presence* of  $I_a$  as shown in Fig. 3(a) for  $T = 30$  K. The results seem to be paradoxical. Finite resistivity should be present only above the magnetically measured IL, which in Fig. 3(a) occurs above 1600 Oe. Below the IL the resistivity should be immeasurable in standard transport measurements. This is indeed the case at low  $I_a$ . However, at elevated currents, substantial  $R$  is measured *concurrently* with the hysteretic magnetization well below the IL [in Fig.

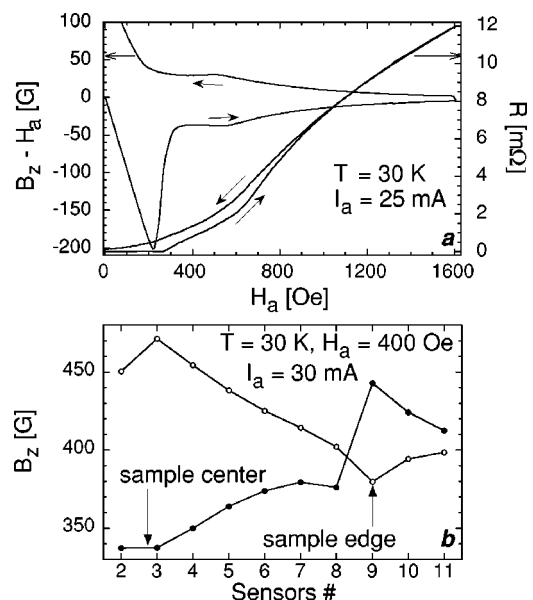


FIG. 3. (a) Resistance (right axis) and hysteretic magnetization loop in the sample center (left axis) vs  $H_a$  at  $T = 30$  K and  $I_a = 25$  mA for crystal B. (b) Profile of magnetic induction across the sample at 400 Oe on increasing (●) and decreasing (○) fields.

3(a)]. Figure 3(b) shows the corresponding field profile  $B_z(x)$  obtained by the Hall sensors at 400 Oe on increasing and decreasing  $H_a$  in presence of  $I_a$ . A clear Bean profile is observed.<sup>14</sup> Fitting this profile to the theoretical  $B_z(x)$  in platelet sample<sup>15</sup> results in critical current density  $J_c = 2 \times 10^4$  A/cm<sup>2</sup>, which translates into total critical current of  $I_c = 4.2$  A. Obviously, a transport current of 25 mA, which is less than 1% of  $I_c$ , cannot result in measurable resistance in the standard critical state models. Figure 2 shows  $I_c(T)$  determined from the Bean profiles together with the  $R(T)$  data. The reentrant resistance always occurs in the region where  $I_a \ll I_c$ . We can also compare the electrical fields. In the magnetization measurements of Fig. 3 the slow sweep of  $H_a$  of about 0.3 Oe/sec induces an average electrical field of  $4 \times 10^{-10}$  V/cm in the sample, which corresponds to a very low vortex velocity of  $10^{-4}$  cm/sec at 400 Oe, for example. The resistively measured electrical field, induced by the simultaneous transport current, on the other hand, is  $1.4 \times 10^{-3}$  V/cm. This translates into vortex velocity of 350 cm/sec, which is six orders of magnitude higher. Clearly, existence of such a high vortex flow rate induced by *concurrently* applied  $I_a$  should have resulted in completely reversible magnetization, in sharp contrast to the data. So paradoxically we have a situation in which a transport current, which is two orders of magnitude *lower* than  $I_c$ , results in vortex velocity which is six orders of magnitude *higher* than the flux creep vortex velocity at  $I_c$ .

We emphasize that we do not observe any heating effects as confirmed by monitoring the location of the resistive transitions at  $T_c$  and  $T_m$  at various currents. Furthermore, and more importantly, since the two measurements are carried out simultaneously, the transport and the magnetization results should be affected by heating to the same extent, and therefore heating effects can be ruled out as a possible explanation of the observed large discrepancy between the two measurements.

We describe the observed phenomena in terms of shear-induced decoupling and shear-enhanced anisotropy. At elevated temperatures in the vortex-liquid phase the in-plane current density  $j_{ab}(z)$  decreases approximately exponentially from the top surface to the bottom.<sup>1</sup> In samples of typical dimensions the current at the bottom is about four orders of magnitude lower than at the top, due to high anisotropy  $\gamma$  of BSCCO. As  $T$  is decreased the pinning becomes more effective. At some temperature the current density at the bottom becomes comparable or lower than  $J_c$ . As a result the vortices at the bottom stop moving or reduce their velocity substantially, whereas the vortices at the top maintain their high velocity since the current density there is significantly above  $J_c$ . As a result, the velocity gradient between the planes  $dv_{ab}/dz$  is increased. The thickness of the vortex pinned layer grows as  $T$  is decreased resulting in progressively larger velocity gradients within the vortex mobile part at the top. The enhanced  $dv_{ab}/dz$  results, in turn, in shear-induced phase slippage between the adjacent CuO<sub>2</sub> planes reducing the Josephson coupling and leading to decoupling of the planes.<sup>3,4</sup> As a result the  $\rho_c$ , and hence the measured  $R$ , are increased significantly causing the reentrant  $R(T)$ . This process is highly nonlinear, since larger  $I_a$  results in larger  $dj_{ab}/dz$ , causing an increase in  $\rho_c$  and  $\gamma$ , which lead in turn to even shallower current profile and thus extremely nonlin-

ear  $R(I)$ . Since the onset of the enhanced shear is induced by pinning, low dose irradiation causes the anomalous behavior to set in at higher  $T$  and lower  $I_a$  as seen in Fig. 1. It is important to realize that the enhanced  $\rho_c$  prevents the lower vortex pinned region from effectively shunting the current. In the case of full decoupling, for example,  $\rho_c$  becomes comparable to the normal state  $\rho_c$ , which in BSCCO crystals of typical dimensions results in about  $10^{-4}$   $\Omega$  resistance between two adjacent CuO<sub>2</sub> planes. Thus the serial  $c$ -axis resistance of several decoupled layers in the upper part of the sample can be of the order of  $10^{-3}$   $\Omega$ , thus effectively insulating the lower zero-resistance region. Any velocity gradient  $dv_{ab}/dz$  should, in principle, completely decouple the layers, since the time-averaged Josephson phase difference reduces to zero. More detailed analysis,<sup>16</sup> however, shows that the pancake shear occurs through a 'stick-slip' process, which retains a finite Josephson coupling at low  $dv_{ab}/dz$ . Thus the Josephson current between the layers can be sustained at low  $dv_{ab}/dz$ , and is lost at higher rates of pancake shear.

The described mechanism is *conceptually* different from conventional electrodynamics in which the dissipation is determined only by the local vortex velocity, and not by the velocity *gradient*. The underlying physics is also very different from the process of nonlocal resistivity,<sup>5,6</sup> in which a force applied to a pancake vortex results in a nonlocal drag of pancakes in adjacent layers. This drag, which is proportional<sup>6</sup> to  $d^2v_{ab}/dz^2$ , induces a more uniform vortex flow, in contrast to the described shear-induced decoupling which has an opposite effect of amplification of the velocity differences.

Since in most of the crystal thickness the vortices are pinned, Bean profiles are obtained in the bulk upon sweeping  $H_a$  [Fig. 3(b)]. At the same time, the transport current, confined to the top planes, is sufficient to create vortex flow in these planes, resulting in a measurable voltage drop, and explaining the apparent discrepancy between the transport and magnetization data. A similar mechanism probably occurs when the  $c$ -axis properties are probed by transverse ac susceptibility and transport in the zero-field-cooled state as reported previously.<sup>17</sup> Our model also explains the hysteretic  $R(H)$  in Fig. 3(a). The field  $B$  in the top planes is determined by the hysteretic Bean profile in the rest of the crystal. As a result, the measured  $R(H_a)$  displays hysteresis, even though the vortices are mobile in the top planes. Consequently, this apparent hysteresis practically disappears when  $R$  is plotted vs the average field  $B$  measured by the sensors, rather than vs  $H_a$ .

Figure 4 summarizes the  $B$ - $T$  diagram of sample A at 30 mA. A similar diagram is obtained for the irradiated crystal B. The resistance vanishes within our resolution at  $T_{R=0}$ , the position of which is highly current dependent. The resistively determined FOT extends to fields of about 500 Oe in this sample. The anomalous reentrant  $R(T)$  is observed in the broad region between  $T_{R=0}$  and  $T_{min}$ , where vortices are pinned in the bulk. It is interesting to note that with increasing  $I_a$ , the shear-induced decoupling process occurs first in the entangled vortex-solid phase<sup>11</sup> above 500 Oe, where vortex cutting is apparently relatively easy. At higher  $I_a$  the decoupling expands also into the quasi-ordered-lattice phase below  $T_m$ , as is the case in Fig. 4. The nonlinearities expand

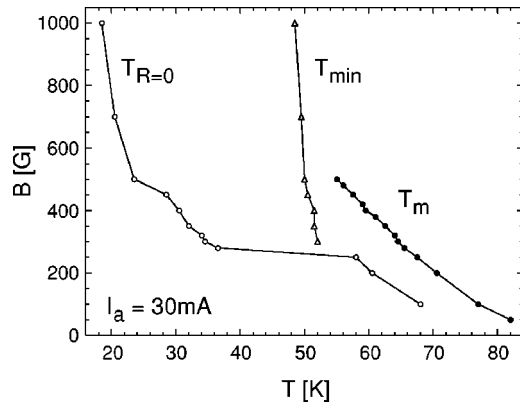


FIG. 4.  $B$ - $T$  phase diagram of crystal A at 30 mA.  $T_m$  (●) is the first-order melting line.  $T_{min}$  (△) is the position of the resistivity minimum, and  $T_{R=0}$  (○) is the temperature at which  $R$  falls below the experimental resolution.

also partially into the liquid phase above  $T_{min}$  and  $T_m$ , where the shear process can still modify  $\rho_c$  at higher currents.

One can evaluate the number of the  $\text{CuO}_2$  planes participating in the flow of vortex pancakes. In Fig. 2(b) at 30 K, for example, the total critical current determined from the Bean profiles is  $I_c = 3.7$  A. This translates into critical current of about 0.18 mA per (double)  $\text{CuO}_2$  plane of the sample. Thus, the top 140 planes would be sufficient to carry the entire  $I_a = 25$  mA without observable dissipation. In order to obtain the large measured resistance the actual current in the planes has to be significantly above 0.18 mA. Furthermore, the lower part of the sample also carries a substantial portion

of  $I_a$ . We therefore conclude that only a few tens of  $\text{CuO}_2$  planes at the top of the crystal participate in the described process. Current-induced decoupling was recently analyzed theoretically in absence of Josephson coupling.<sup>16</sup> It was found that above some critical value of the current applied to the top plane, slippage between magnetically coupled planes occurs, leading to an abrupt increase in the vortex velocity in the top plane. Since in this model  $\rho_c$  is infinite, there is no corresponding current redistribution. Computer simulations<sup>18</sup> of Josephson-coupled planes also show sharp current-induced decoupling. Vortex cutting was also observed in YBCO crystals at elevated currents in flux transformer measurements.<sup>19,20</sup> The much lower anisotropy of YBCO, however, causes only a small change in the transport properties. In BSCCO in contrast the shear-induced decoupling leads to variations by orders of magnitude in the observed behavior.

In conclusion, we reveal large apparent discrepancies between simultaneously measured magnetization and transport properties, which reveal an important feature of vortex dynamics in the presence of inhomogeneous currents. In layered superconductors at elevated currents the  $c$ -axis resistivity becomes a strong function of the local current gradient  $dj_{ab}/dz$ , instead of being determined just by the current density. This mechanism results in a highly nonlinear reentrant resistance well below the irreversibility line.

This work was supported by Israel Ministry of Science, by U.S.-Israel Binational Science Foundation (BSF), by the German-Israeli Foundation (GIF), by CREST, and by the Grant-in-Aid for Scientific Research from the Ministry of Education, Science, Sports and Culture, Japan.

\*Present address: Quantum Institute, University of California, Santa Barbara, CA 93106.

†Present address: National Research Institute for Metals, Sengen 1-2-1, Tsukuba 305-0047, Japan.

<sup>1</sup>R. Busch *et al.*, Phys. Rev. Lett. **69**, 522 (1992).

<sup>2</sup>H. Safar *et al.*, Phys. Rev. B **46**, 14 238 (1992).

<sup>3</sup>E. H. Brandt, Rep. Prog. Phys. **58**, 1465 (1995).

<sup>4</sup>A. E. Koshelev, Phys. Rev. Lett. **76**, 1340 (1996).

<sup>5</sup>G. Blatter *et al.*, Rev. Mod. Phys. **66**, 1125 (1994).

<sup>6</sup>D. A. Huse and S. N. Majumdar, Phys. Rev. Lett. **71**, 2473 (1993).

<sup>7</sup>S. Ooi *et al.*, Physica C **302**, 339 (1998).

<sup>8</sup>E. Zeldov *et al.*, Nature (London) **375**, 373 (1995).

<sup>9</sup>D. T. Fuchs *et al.*, Nature (London) **391**, 373 (1998).

<sup>10</sup>D. T. Fuchs *et al.*, Phys. Rev. Lett. **81**, 3944 (1998).

<sup>11</sup>B. Khaykovich *et al.*, Phys. Rev. B **56**, R517 (1997).

<sup>12</sup>S. Bhattacharya and M. J. Higgins, Phys. Rev. Lett. **70**, 2617 (1993).

<sup>13</sup>W. K. Kwok *et al.*, Phys. Rev. Lett. **73**, 2614 (1994).

<sup>14</sup>The curvature of the profile near the sample edge on increasing field is due to surface barriers, see for example E. Zeldov *et al.*, Europhys. Lett. **30**, 367 (1995).

<sup>15</sup>E. H. Brandt and M. Indenbom, Phys. Rev. B **48**, 12 893 (1993); E. Zeldov *et al.*, *ibid.* **49**, 9802 (1994).

<sup>16</sup>T. Pe, M. Benkraouda, and J. R. Clem, Phys. Rev. B **55**, 6636 (1997); **56**, 8289 (1997).

<sup>17</sup>E. Rodriguez *et al.*, Phys. Rev. Lett. **71**, 3375 (1993).

<sup>18</sup>W. Yu and D. Stroud, Phys. Rev. B **51**, 3725 (1995); K. K. Uprety and D. Dominguez, *ibid.* **51**, 5955 (1995).

<sup>19</sup>H. Safar *et al.*, Phys. Rev. Lett. **72**, 1272 (1994).

<sup>20</sup>D. Lopez *et al.*, Phys. Rev. B **50**, R9684 (1994); Physica C **260**, 211 (1996).